Thermal decomposition of iso-propanol: First-principles prediction of total and product-branching rate constants

B. H. Bui, R. S. Zhu, and M. C. Lin

Citation: The Journal of Chemical Physics **117**, 11188 (2002); doi: 10.1063/1.1522718
View online: http://dx.doi.org/10.1063/1.1522718
View Table of Contents: http://scitation.aip.org/content/aip/journal/jcp/117/24?ver=pdfcov
Published by the AIP Publishing

Thermal decomposition of iso-propanol: First-principles prediction of total and product-branching rate constants

B. H. Bui, R. S. Zhu, and M. C. Lin[a)]
Department of Chemistry, Emory University, Atlanta, Georgia 30322

(Received 12 August 2002; accepted 30 September 2002)

The unimolecular decomposition of iso-C_3H_7OH has been studied with a modified GAUSSIAN-2 method. Among the six low-lying product channels identified, the H_2O-elimination process (2) via a four-member-ring transition state is dominant below 760 Torr over the temperature range 500–2500 K. At higher pressures and over 1200 K, the cleavage of a C-C bond by reaction (1) producing $CH_3+CH_3C(H)OH$ is predicted to be dominant. The predicted low- and high-pressure limit rate constants for these two major product channels can be given by $k_1^0=6.3\times10^{42}\,T^{-16.21}\exp(-47\,400/T)$, $k_2^0=7.2\times10^{44}\,T^{-14.70}\exp(-35\,700/T)\,\mathrm{cm^3\,molecule^{-1}\,s^{-1}}$, $k_1^\infty=8.0\times10^{29}\,T^{-3.75}\exp(-45\,800/T)$, and $k_2^\infty=2.0\times10^{6}\,T^{2.12}\exp(-30\,700/T)\,\mathrm{s^{-1}}$, respectively. Predicted k_1 values compare reasonably with available experimental data; however, k_2 values are lower than the experimentally determined apparent rate constant for C_3H_6 formation, which may derive in large part from secondary radical reactions. Other minor decomposition products were predicted to have the barriers $H_2+CH_3C(O)CH_3$, $E_3^0=82.8$ kcal/mol; $H_2O+{}^1CH_3CCH_3$, $E_4^0=77.9$ kcal/mol; $CH_4+CH_3C(H)O$, $E_5^0=84.3$ kcal/mol; and $CH_4+{}^1CH_3COH$, $E_6^0=81.9$ kcal/mol. The triplet-singlet energy gap for CH_3CCH_3 was predicted to be 5.2 kcal/mol, favoring the singlet state. © *2002 American Institute of Physics.* [DOI: 10.1063/1.1522718]

I. INTRODUCTION

Isopropanol (IPA, 2-C_3H_7OH) is a potential fuel additive for use in internal and Diesel combustion engines. Although the kinetics and mechanism for its thermal decomposition reaction have been investigated with conventional static reactors by several authors,[1–3] existing data to date are incomplete and conflicting. Barnard[1] first reported that the major decomposition products were H_2 and CH_3COCH_3 with smaller amounts of H_2O and CH_4. The overall rate of decomposition could be effectively inhibited by NO, a well-known free radical scavenger; accordingly, a radical decomposition mechanism initiated by breaking the secondary C–H bond was proposed to account for the findings. Maccoll and Thomas[2] asserted that, although the decomposition reaction might be dominated by radical reactions, under a fully NO-inhibited condition the molecular H_2O-elimination mechanism prevailed and the formation of $H_2O+C_3H_6$ (propene) was found to occur with 64.5 kcal/mol activation energy.

Trenwith[3] subsequently investigated the decomposition reaction in greater detail employing a KCl-coated quartz reactor to minimize potential surface effects. He confirmed mostly Barnard's observations that under essentially homogeneous conditions, the pyrolysis of 10–100 Torr iso-C_3H_7OH in the temperature range 721–801 K produced primarily $H_2+CH_3COCH_3$ with smaller amounts of H_2O and C_3H_6 and traces of CH_4, C_2H_6, C_2H_4, and CH_3CHO. A radical mechanism initiated by splitting a C–C bond producing CH_3 and CH_3CHOH was proposed.[3] The two key product pairs $H_2+CH_3COCH_3$ and $H_2O+C_3H_6$ were assumed to have resulted from the following chain processes:

$$X+C_3H_7OH\rightarrow HX+CH_3C(OH)CH_3 \quad \text{and} \quad CH_3CH(OH)CH_2,$$

$$CH_3C(OH)CH_3\rightarrow H+CH_3COCH_3,$$

$$CH_3CH(OH)CH_2\rightarrow OH+C_3H_6,$$

where $X=$H, OH, and CH_3, key chain carriers in the system produced by the initiation as well as the chain reactions. The molecular dehydration reaction put forth by Maccoll and Thomas[2] was concluded to be unimportant under the conditions employed.[3] For the C–C bond breaking reaction suggested by Trenwith, Tsang[4] has estimated the unimolecular rate constant to be $k_1=3.16\times10^{16}e^{-41\,100/T}\,\mathrm{s^{-1}}$; this result will be compared with our predicted value later.

The conclusions reached by Barnard[1] and Trenwith[3] contradict, to some extent, the results of our recent experimental and theoretical studies on the decomposition of small alcohols[5,6] that both the H_2O-molecular elimination and radical decomposition processes take place concurrently, with the former process dominating at lower temperatures and the latter dominating at higher temperatures. This is true even for CH_3OH, which has been shown to produce both ${}^1CH_2+H_2O$ and the commonly assumed CH_3+OH products, with the former being dominant under the atmospheric combustion condition.[6] More recently, Shu *et al.* studied the decomposition of chemically activated C_3H_7OH by the $O({}^1D)+C_3H_8$ reaction in a cross-molecular beam experiment.[7] A direct comparison of this new result with the aforementioned data is difficult in view of the fact that in addition to the

a)Corresponding author: National Science Council Distinguished Visiting Professor at Chiaotung University, Hsinchu, Taiwan. Electronic mail: chemmcl@emory.edu

direct H-abstraction processes both n-C_3H_7OH and iso-C_3H_7OH could be produced in this beam experiment.

In order to fully examine the kinetics and mechanism for this basically and practically important chemical system, we have carried out a full mapping of the potential-energy surface (PES) of the system with the modified GAUSSIAN-2 (G2M) method.[8] We have also calculated the rate constants for low-lying reaction channels for comparison with available kinetic data mentioned above.

II. COMPUTATIONAL METHODS

A. *Ab initio* calculations

The hybrid density functional method (B3LYP) with the 6-311G(d,p) basis set has been used to optimize the geometry of the reactant, transition states and products.[9–11] The intrinsic reaction coordinate[12] (IRC) calculations were utilized to confirm the connection between a transition state and a designated intermediate. The same level of theory was applied to calculate the vibrational frequencies of all species in each reaction pathway. These values would be employed for zero-point energy (ZPE) corrections, characterization of the nature of stationary points, and rate constant calculations.

Higher-level single-point calculations were also carried out with the optimized geometries using the modified GAUSSIAN-2 (G2M) (Ref. 8) method to achieve a more reliable evaluation of energies. The applied model G2M(CC5) (Ref. 8) uses a series of calculations with the B3LYP/6-311G(d,p) optimized geometries to approximate the CCSD(T)/6-311+G($3df,2p$) level of theory, including a ''higher level correction'' (HLC) based on the number of paired and unpaired electrons. The following is a summary of the G2M scheme:[8]

$$E_{\text{base}} = E[\text{PMP4/6-311G}(d,p)],$$

$$\Delta E(\text{CC}) = E[\text{CCSD(T)/6-311G}(d,p)] - E_{\text{base}},$$

$$\Delta E(+3df2p) = E[\text{MP2/6-311+G}(3df,2p)] - E[\text{MP2/6-311G}(d,p)],$$

$$\Delta E(\text{HLC,CC5}) = -5.30n_\beta - 0.19n_\alpha,$$

$$E[\text{G2M(CC5)}] = E_{\text{base}} + \Delta E(\text{RCC}) + \Delta E(+3df2p) + \Delta E(\text{HLC,CC5}) + \text{ZPE},$$

where n_α and n_β are the numbers of valence electrons, $n_\alpha \geqslant n_\beta$. All calculations were carried out with the GAUSSIAN 98 program.[13]

B. RRKM calculations

Rate constants were computed with a microcanonical variational RRKM method using the VARIFLEX code.[14] The pressure dependence of the rate constant was treated by one-dimensional (1D) master equation calculations using the Boltzmann probability of the complex for the J distribution. The master equation was solved by an eigenvalue-solver-based approach for the dissociation processes.[15,16] In order to achieve convergence in the integration over the energy range, an energy grain size of 120 cm^{-1} was used: this grain size provides numerically converged results for all temperature studies with the energy spanning the range from 30 418 cm^{-1} below to 65 582 cm^{-1} above the threshold forming $CH_3 + CH_3C(H)OH$. The total angular momentum J covered the range from 1 to 241 in steps of 10 for the E, J-resolved calculation. For the barrierless transition states, the Morse potential

$$V(R) = D_e\{1 - \exp[-\beta(R - R_e)]\}^2$$

was used to represent the potential energy along the individual reaction coordinate. For the tight transition states, the numbers of states were evaluated according to the rigid-rotor harmonic-oscillator assumption.

III. RESULTS AND DISCUSSION

A. Potential-energy surface of the system

The optimized geometries of the reactant (IPA), intermediates, transition states, and some of the products are shown in Fig. 1 including the characteristic bond distances and angles. Figure 2 shows the potential-energy surface obtained at the G2M level. Table I displays details of relative energies obtained at various theoretical levels of calculation. The vibrational frequencies and moments of inertia of important species used in the rate constant calculations are presented in Table II. As shown in the PES (Fig. 2), the decomposition of IPA can occur through many product channels:

$$2\text{-}C_3H_7OH \rightarrow CH_3C(H)OH + CH_3 \quad (1)$$

$$\rightarrow CH_3C(H)CH_2 + H_2O \quad (2)$$

$$\rightarrow CH_3C(O)CH_3 + H_2 \quad (3)$$

$$\rightarrow {}^1CH_3CCH_3 + H_2O \quad (4)$$

$$\rightarrow CH_3C(H)O + CH_4 \quad (5)$$

$$\rightarrow {}^1CH_3COH\text{-}cis + CH_4 \quad (6)$$

$$\rightarrow (CH_3)_2COH + H \quad (7)$$

$$\rightarrow CH_3C(H)CH_3 + OH \quad (8)$$

$$\rightarrow CH_2C(OH)CH_3 + H_2. \quad (9)$$

We have calculated the heats of reaction at 0 and 298.15 K for several important products channels as presented in Table III. The predicted values are compared with the experimental heats of reaction using available experimental heats of formation.[17,18] As shown in Table III, the deviations between the predicted and experimental heats of reaction at 0 K, $\Delta\Delta H_{rxn}$ (0 K) are within the expected errors of the G2M method, which has a average absolute error of about 1.2 kcal/mol for the molecular species consisting of elements in the first two rows of the periodic table.[8] In the worst case, the $\Delta\Delta H_{rxn}$ (0 K) for the reaction $2\text{-}C_3H_7OH \rightarrow CH_3 + CH_3C(H)OH$ is 3.6 kcal/mol, which is beyond the reliability of the G2M method. This prompted us to calculate the heat of formation of the $CH_3C(H)OH$ radical, whose experimental value of $\Delta_f H^0_{298}$ was reported to be -15.2 ± 1.0 kcal/mol,[18] using the isodesmic reaction $2\text{-}C_3H_7OH + CH_2OH \rightarrow CH_3C(H)OH + C_2H_5OH$. The new value

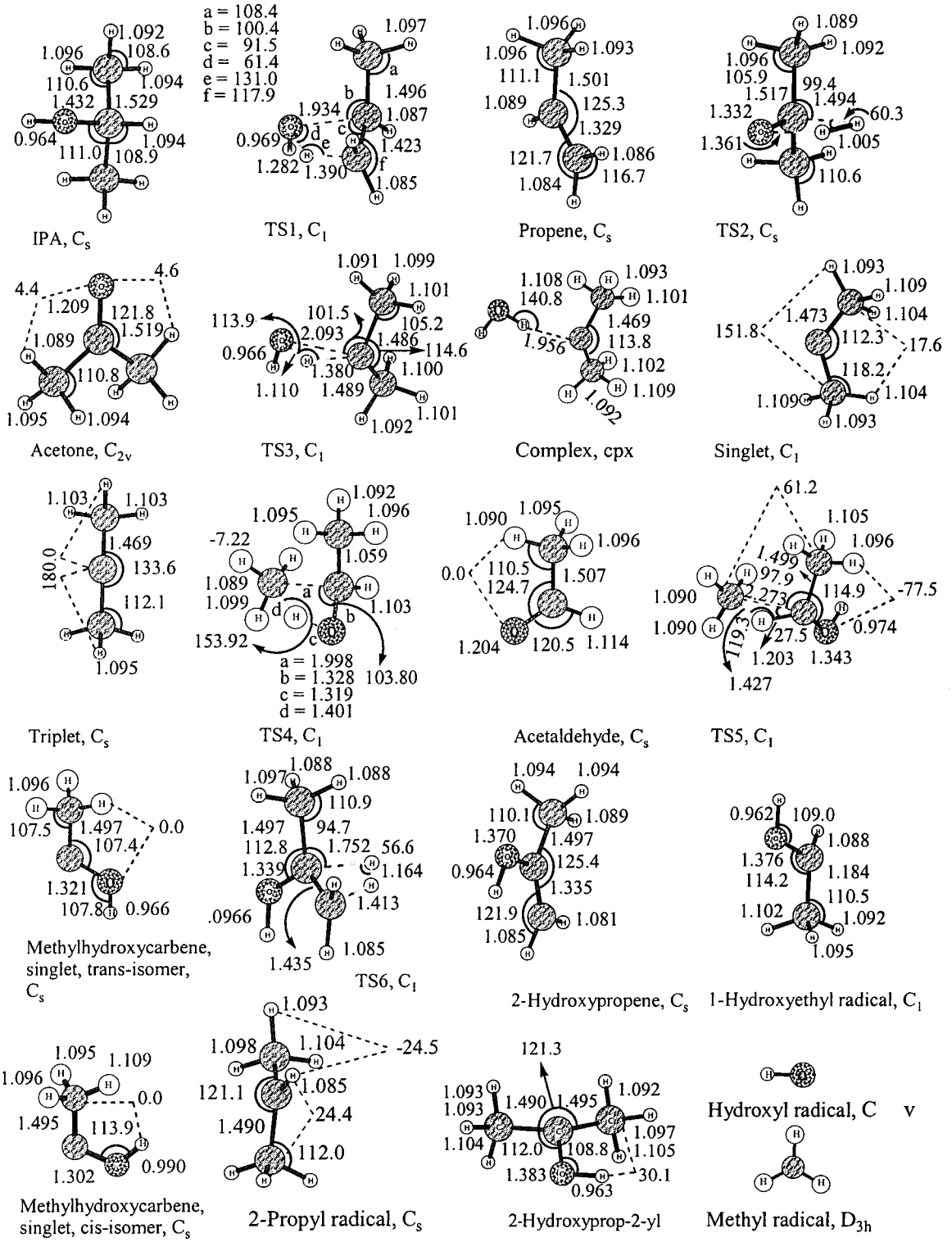

FIG. 1. Optimized geometries of the reactant, transition states, and products computed at the B3LYP/6-311(d,p) level.

$\Delta_f H^0_{298} = -13.3$ kcal/mol for $CH_3C(H)OH$ gave rise to a much smaller deviation $\Delta\Delta H_{rxn}$ (0 K)=1.7 kcal/mol, which is within the reliability of the G2M method.

The reaction paths for channels (1)–(6) shown in Fig. 2 will be discussed sequentially in the following sections, while the higher energy processes (7)–(9) will not be included in our rate constant calculation.

$CH_3C(H)OH + CH_3$. Trenwith[3] proposed this radical formation channel as the chain initiator which resulted in the formation of the two key products detected in his experiment: H_2 and $CH_3C(O)CH_3$ and, to a smaller extent, H_2O and $CH_3C(H)CH_2$ as alluded to in the Introduction. For this C–C bond breaking reaction, Tsang[4,19] has estimated the unimolecular rate constant to be $k_1 = 3.2\times10^{16} e^{-41\,100/T}\,s^{-1}$, with 82 kcal/mol activation energy. Due to the absence of a well-defined transition state for the fragmentation reaction

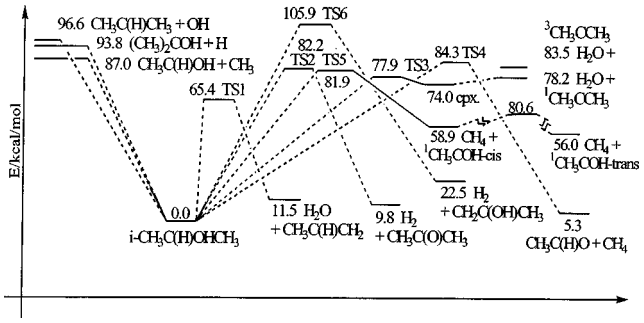

FIG. 2. Schematic energy diagram for the dissociation of IPA computed at the G2M(CC5) level.

producing $CH_3C(H)OH+CH_3$, its dissociation potential function was computed variationally to cover a range of C–C separations from the equilibrium value 1.529 Å to 3.5 Å with an interval of 0.2 Å. At the B3LYP/6-311G(d,p) level of theory, we optimized every structure at each interval of the C–C bond separation and also calculated the 3N-7 vibrational frequencies, projected out of the gradient direction. In this manner, a smooth and reasonable potential curve in terms of total energy at each point along the reaction path was obtained and used to evaluate the Morse potential energy function and then scaled to match the dissociation energy predicted at the G2M level of theory. The potential energy function $V(R)$ given above was obtained with $D_e=86.3$ kcal/mol, $\beta=2.031$ Å^{-1}, and $R_e=1.529$ Å, which is the equilibrium value of R, i.e., the equilibrium C–C bond length in iso-C_3H_7OH structure. This potential for the dissociation process was used in all subsequent RRKM calculations. The dissociation energy for channel (1) as predicted at the G2M level is 87.0 kcal mol^{-1} and is 5 kcal/mol higher than the activation energy reported by Tsang for temperature above 1050 K.[4]

$CH_3C(H)CH_2+H_2O$. The result presented in Fig. 1 shows that H_2O elimination from IPA occurs via a four-centered-ring TS1 with C_1 symmetry. The dihedral angle of the H atom in this ring, HCCO, is 0.7°, which is closer to the values 0.2° and 1.7° obtained in similar structures for the decomposition of C_2H_5OH by Park *et al.*[5] and Butkovskaya and co-workers,[20] respectively. Also, the out-of-ring H atom is largely bent away from the HCCO ring with a dihedral angle of HOCC at 105.2° which is not much different from the reported values 107.4° (Ref. 5) and 101.17° (Ref. 20) for ethanol. The breaking C–O and C–H bonds in TS1 are 0.502 and 0.294 Å longer than those in IPA, respectively. The corresponding deviations calculated in the similar H_2O-elimination process in C_2H_5OH are 0.433 and 0.340 Å.[5] TS1 represents a well-defined transition structure, whose energy (G2M) is 65.4 kcal mol^{-1}, leading to the formation of water and propene from IPA. Our reported value is about 7.2 kcal/mol higher than the apparent activation energy for C_3H_6 formation,[3] 58.2±3.5 kcal mol^{-1}; however, it is close to the value 64.5 kcal/mol obtained by Maccoll and Thomas under fully NO-inhibited conditions.[2] It is worth noting that the similar H_2O-elimination transition state (TS1) of the C_2H_5OH system[5] has an energy barrier of 66.6 kcal/mol at the G2M(RCC2) level.

$CH_3C(O)CH_3+H_2$. As shown in Fig. 1, the formation of the H_2 molecule occurs via a four-centered TS2 with C_s symmetry, involving of the H atom and the OH group attached to the center C atom. In TS2, the HHOC ring is planar with a dihedral of 0.0°; the breaking C–H and O–H bonds lengthen from 1.094 and 0.964 Å in IPA to 1.494 and 1.361 Å, respectively. The forming H_2 bond 1.005 Å is much longer than the H_2 molecular equilibrium bond length 0.744 Å predicted at the same level of theory. A similar transition state for H_2 elimination in C_2H_5OH (Ref. 5) was found to be close to TS2 of IPA in term of bond lengths

TABLE I. Relative energies (in kcal/mol^{-1}) of species calculated at various theoretical levels.

Species	ΔZPE[b]	B3LYP/ 6-311G(d,p)	PMP4/ 6-311G(d,p)	CCSD(T)/ 6-311G(d,p)	MP2 /6-311G(d,p)	MP2/ 311+G$(3df,2p)$	G2M
IPA[a]	0	−194.41845	−193.90633	−193.90623	−193.83854	−193.96168	−193.99238
TS1	−5.25	66.58	72.35	73.44	72.85	70.03	65.38
$C_3H_6+H_2O$	−4.44	16.91	19.68	18.77	19.55	16.72	11.50
TS2	−6.09	86.54	90.01	91.34	91.13	88.08	82.21
$CH_3C(O)CH_3+H_2$	−9.14	16.22	17.54	18.67	19.12	19.34	9.76
TS3	−5.75	79.07	85.09	84.66	87.87	86.89	77.93
cpx	−5.10	76.22	82.07	80.67	84.48	82.90	73.98
$^1CH_3CCH_3+H_2O$	−7.12	85.19	89.76	87.94	92.56	89.92	78.17
$^3CH_3CCH_3+H_2O$	−6.71	84.70	88.33	86.69	89.09	89.44	83.50
TS4	−5.77	87.24	91.59	93.18	92.42	89.26	84.25
$CH_3C(H)O+CH_4$	−4.97	4.92	8.64	9.53	10.58	11.27	5.26
TS5	−5.31	83.12	88.61	88.29	91.23	90.12	81.87
$^1CH_3C(OH)$-*cis*$+CH_4$	−5.78	59.72	65.35	64.38	69.57	69.90	58.93
$^1CH_3C(OH)$-*trans*$+CH_4$	−5.15	56.67	61.28	60.52	65.33	65.91	55.95
TS6	−7.50	108.76	115.12	115.19	116.22	114.41	105.9
$CH_2CO(H)CH_3+H_2$	−8.31	28.97	32.60	32.45	32.91	31.32	22.56
$CH_3C(H)OH+CH_3$	−7.73	85.01	92.68	91.08	94.95	95.44	87.02
$(CH_3)_2COH+H$	−8.70	96.89	99.43	98.72	98.21	98.81	93.80
$CH_3C(H)CH_3+OH$	−7.38	93.98	98.65	96.66	103.22	107.37	96.62

[a]The ZPE at the B3LYP/6-311G(d,p) level and total energies at other levels for IPA are given in units of a.u.
[b]ZPE are calculated at the B3LYP/6-311G(d,p) level and only included in the G2M energy. ΔZPE represents the ZPE relative to that of IPA.

TABLE II. Moments of inertia (I_A,I_B,I_C) and vibrational frequencies of the species involved in the iso-C_3H_7OH decomposition reaction computed at the B3LYP/6-311G(d,p) level.

Species	I_i (a.u.)	ν_j (cm^{-1})
IPA	212.6, 226.3, 380.6	233, 273, 312, 360, 429, 472, 814, 922, 939, 964, 1091, 1146, 1184, 1315, 1363, 1399, 1414, 1427, 1484, 1485, 1499, 1507, 3012, 3016, 3043, 3073, 3085, 3103, 3106, 3806
$CH_2CO(H)CH_3$	178.6, 198.7, 366.1	182, 480, 808, 1022, 1365, 1472, 3032, 3139, 409, 505, 862, 1075, 1415, 1493, 3081, 3235, 438, 726, 980, 1210, 1452, 1719, 3131, 3816
$CH_3C(H)CH_3$	48.1, 217.1, 242.8	103, 395, 945, 1178, 1413, 1480, 2937, 3082, 115, 883, 1028, 1367, 1469, 1492, 3011, 3083, 353, 939, 1146, 1408, 1478, 2932, 3012, 3163
$CH_3C(H)OH$	40.7, 191.9, 219.4	205, 362, 409, 601, 915, 1021, 1063, 1202, 1310, 1401, 1439, 1468, 1486, 2928, 3004, 3094, 3181, 3814
$(CH_3)_2COH$	194.1, 222.8, 389.5	168, 189, 326, 366, 377, 431, 792, 953, 977, 1008, 1088, 1143, 1302, 1375, 1411, 1420, 1464, 1477, 1485, 1494, 2915, 2930, 3019, 3056, 3092, 3103, 3828
TS1	213.2, 262.9, 410.7	1996 *i*, 214, 285, 322, 395, 427, 529, 597, 785, 848, 905, 953, 1013, 1102, 1205, 1247, 1390, 1427, 1435, 1470, 1492, 1506, 1608, 3019, 3094, 3110, 3127, 3146, 3194, 3761
TS2	205.9, 228.7, 377.0	2200 *i*, 203, 247, 370, 444, 507, 678, 775, 820, 908, 969, 1038, 1056, 1149, 1255, 1371, 1393, 1402, 1460, 1473, 1478, 1494, 1878, 2113, 3026, 3032, 3096, 3104, 3139, 3140
TS3	219.9, 305.0, 473.7	829 *i*, 168, 189, 220, 257, 403, 414, 591, 727, 817, 871, 1003, 1077, 1181, 1210, 1374, 1380, 1432, 1452, 1480, 1505, 1550, 1973, 2966, 2972, 3016, 3024, 3085, 3109, 3810
TS4	211.1, 268.4, 421.4	2135 *i*, 103, 241, 267, 435, 478, 537, 569, 744, 884, 939, 1011, 1128, 1178, 1229, 1304, 1386, 1430, 1438, 1463, 1471, 1485, 2025, 2939, 3009, 3026, 3095, 3120, 3131, 3172
TS5	209.9, 312.3, 462.4	1191 *i*, 91, 208, 224, 266, 463, 585, 623, 678, 721, 932, 1051, 1067, 1117, 1246, 1316, 1381, 1406, 1437, 1469, 1471, 1478, 2283, 2919, 3041, 3044, 3121, 3163, 3173, 3587
TS6	203.3, 221.2, 372.0	2371 *i*, 234, 272, 389, 396, 443, 550, 580, 689, 749, 878, 969, 1038, 1080, 1195, 1311, 1368, 1384, 1403, 1449, 1473, 1483, 1511, 1726, 3021, 3122, 3127, 3166, 3232, 3794

and angles, except that the latter has an energy barrier (82.2 kcal/mol), which is 3.9 kcal/mol lower than that of the former (86.1 kcal/mol) at the G2M level. The 82-kcal/mol H_2-elimination barrier in IPA is much higher than the apparent activation energy reported for H_2 production by Trenwith, 57.6±1.7 kcal/mol, thanks to the contributions from secondary chain reactions: $H+C_3H_7OH \rightarrow H_2+CH_3C(OH)CH_3$, $CH_3C(OH)CH_3 \rightarrow H+CH_3C(O)CH_3$.[3]

$^1CH_3CCH_3+H_2O$. Channel (4) is characterized by the formation of a molecular complex *cpx* via TS3. TS3 is a three-centered ring transition state with C_1 symmetry, which involves the H atom and the OH group attached to the center C atom. The breaking C–O bond is 2.093 Å with respect to the equilibrium bond length 1.432 Å of IPA; the breaking C–H bond (1.380 Å) is 0.286 Å longer than that of the IPA,

TABLE III. Heats of reaction of major channels in the decomposition of 2-propanol.

Reactions	Predicted results (G2M)		Experimental results		Energetic differences
	ΔH_{rxn} (0 K)	ΔH_{rxn} (298 K)	ΔH_{rxn} (0 K)	ΔH_{rxn} (298 K)	$\Delta\Delta H_{rxn}$ (0 K)
$2\text{-}C_3H_7OH \rightarrow H_2O+C_3H_6$	11.5	13.0	10.6	12.1	0.9
$\rightarrow H_2+CH_3C(O)CH_3$	9.8	11.3	*11.5*	*13.3*	−1.7
$\rightarrow CH_4+{}^1CH_3C(OH)$	5.3	6.7	6.3	7.6	−1.0
$\rightarrow CH_3+CH_3C(H)OH$[a]	87.0	88.9	85.3(83.9)	87.0(85.0)	1.7(3.6)
$\rightarrow OH+CH_3C(H)CH_3$	96.6	98.6	*94.0*	*95.7*	2.6

[a]$\Delta_f H^0_{298}(CH_3C(H)OH) = -13.3$ kcal/mol was obtained by using the isodesmic reaction $2\text{-}C_3H_7OH+CH_2OH \rightarrow CH_3C(H)OH+C_2H_5OH$. The experimental value (−15.2 kcal/mol) (Ref. 18) yields another set of ΔH_{rxn} and $\Delta\Delta H_{rxn}$ reported in parentheses.

1.094 Å. The three-centered ring is characterized by the OHC angle 113.9°, which is flattening toward the formation of the complex with the new OHC angle of 140.8°. The out-of-plane bend angle of the OH bond with respect to the ring is found to be almost perpendicular (94.9°). This second H_2O-elimination process producing the singlet dimethyl carbene through the *cpx* complex has a much larger barrier than the first H_2O elimination by TS1. At the G2M level, the barrier of TS3, 77.9 kcal/mol, is 12.5 kcal/mol higher than that of TS1. This can be attributed to the high endothermicity of the process and, to a smaller extent, the strain of the three-centered ring in TS3. The existence of *cpx* is similar to those found in the decomposition of $CH_3OH(H_2C\cdots OH_2)$ and $C_2H_5OH(CH_3CH\cdots OH_2)$.

The C–O bond distance of the *cpx* (2.788 Å) is 0.70 Å longer than that in TS3 (2.093 Å). The energy of the complex relative to the reactant is 74.0 kcal mol^{-1}. The dissociation of the *cpx* yields $^1CH_3CCH_3+H_2O$ barrierlessly with an overall endothermocity of 78.2 kcal mol^{-1}. The energy difference between the lowest singlet and triplet states (S-T gap) of dimethyl carbene (DMC) is also computed and reported here along with other theoretical[21] results and experimental[22] findings. Our predicted S-T gap is 5.3 kcal/mol in favor of the singlet state, which may be compared with the smaller value 1.64 kcal/mol obtained by Matzinger and Fuelscher[21] at the MRCI+Q level; they also indicated that the S-T gap might be 1.0–1.5 kcal/mol larger. Modarelli *et al.*[22] were able to generate and trap the singlet DMC by laser flash photolysis of dimethyldiazairine and using pyridine as chemical trap, respectively. The reduction of pyridinium ylide's yield upon treatment with oxygen indicated a possible intersystem crossing between the singlet and triplet DMC. The authors assumed this interconversion occurs only at a short singlet-triplet splitting, which may be closer to zero.[22]

$CH_3C(H)O+CH_4$. This path involves the abstraction of the H atom from the OH group by CH_3 producing $CH_3C(H)O+CH_4$ through TS4. In this process, the lengthening of a C–C bond followed by the migration of the H atom in the OH group to the CH_3 group results in a twisted four-centered transition state TS4, whose dihedral angle of the ring CCOH is −7.22°, with the cleaving C–C and O–H bonds lengthened by 0.469 and 0.355 Å, respectively, compared with those in the IPA. The forming C–H bond is 1.401 Å, which is much shorter than that of the corresponding TS (1.910 Å) (Ref. 5) in the ethanol system. The result of IRC (Ref. 12) calculation confirms that TS4 connects the IPA and the products $CH_3C(H)O+CH_4$; TS4 lies above IPA by 84.3 kcal/mol.

cis-$^1CH_3COH+CH_4$. As shown in Fig. 1, the H atom on the centered C in IPA can migrate toward the C atom in one of the CH_3 groups to produce *cis*-$^1CH_3COH$ and CH_4 via a three-center transition state TS5 having a barrier of 81.9 kcal/mol, which is 2.4 kcal/mol lower than that of the analogous channel described above. In the decomposition of C_2H_5OH,[5] the energy difference between the two analogous CH_4-elimination channels giving CH_2O and HCOH, respectively, was 14 kcal/mol.[5] The higher energy difference in the C_2H_5OH case may be attributed to a large rotation of $HOCH_2$ moiety observed in the transition state leading to CH_2O. IRC[12] calculations were performed to confirm the connection between TS5 and the products *cis*-$^1CH_3COH$ and CH_4 because the existence of the *trans*-$^1CH_3COH$ conformer, which is more stable than the *cis*-isomer by 2.9 kcal/mol. The internal rotation barrier from *trans* to *cis* was predicted to be 24.6 kcal/mol, which is close to the values 27.3 and 29.7 kcal/mol calculated by Yadav and Goddard[23] and Rasanen *et al.*,[24] respectively.

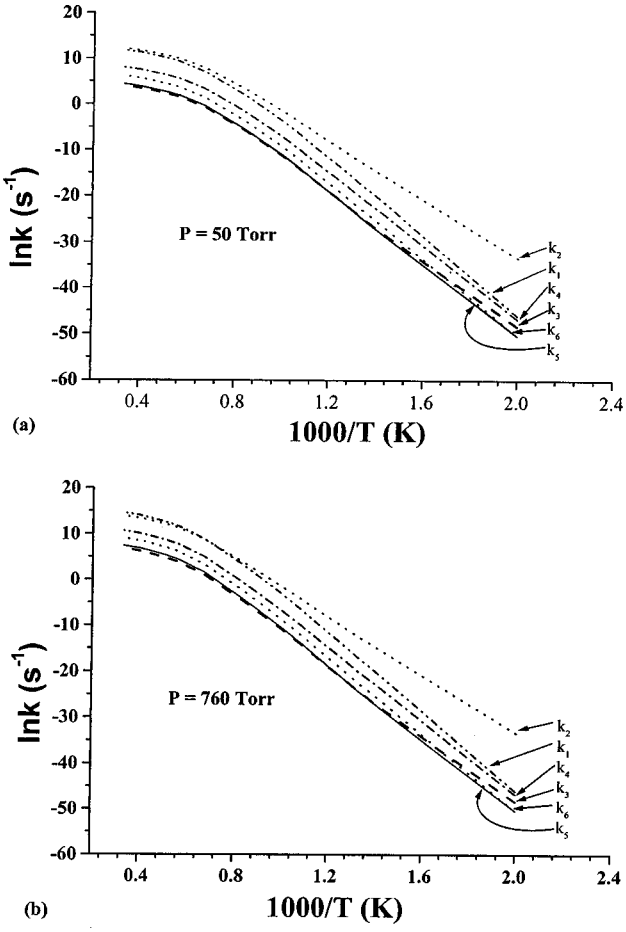

FIG. 3. Predicted rate constants for the dissociation reactions (1)–(6) at 50 Torr (a) and 1 atm (b). The numbers in the figure correspond to reaction channels given in the text.

In Fig. 1, we also show another H_2-elimination transition state TS6 in which the H atom on the center C approaches one of the H atoms in a CH_3 group to eliminate an H_2 molecule. This process has a larger barrier 105.9 kcal/mol and should be unimportant kinetically.

B. Rate constant calculations

For the unimolecular decomposition of 2-C_3H_7OH via various major product channels (1)–(6) discussed above, we utilized the VARIFLEX code of Klippenstein *et al.*[14] to compute the rate constants. The Lennard-Jones parameters for 2-C_3H_7OH and Ar employed in the calculation, σ=4.739 and 3.465 Å and ε/k=456.0 and 113.5 K, respectively, were taken from Ref. 25. The energy transfer per downward collision, $\langle \Delta E_{\text{down}} \rangle$, was assumed to be 400 cm^{-1}. The energies

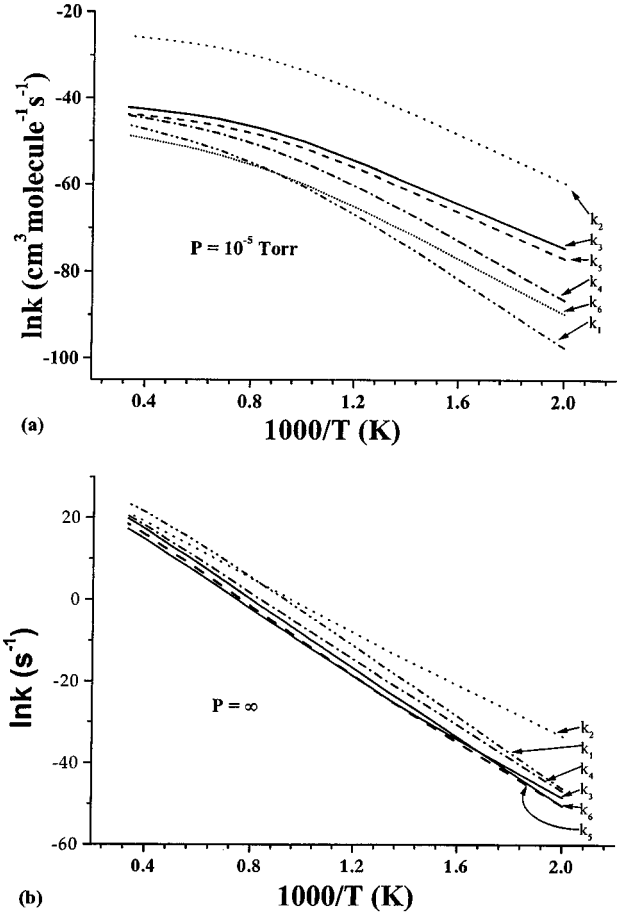

FIG. 4. Predicted temperature dependence of rate constants at the low-pressure (a) and high-pressure, and (b) limits for the dissociation reactions (1)–(6). The numbers in the figure are the same as in Fig. 3.

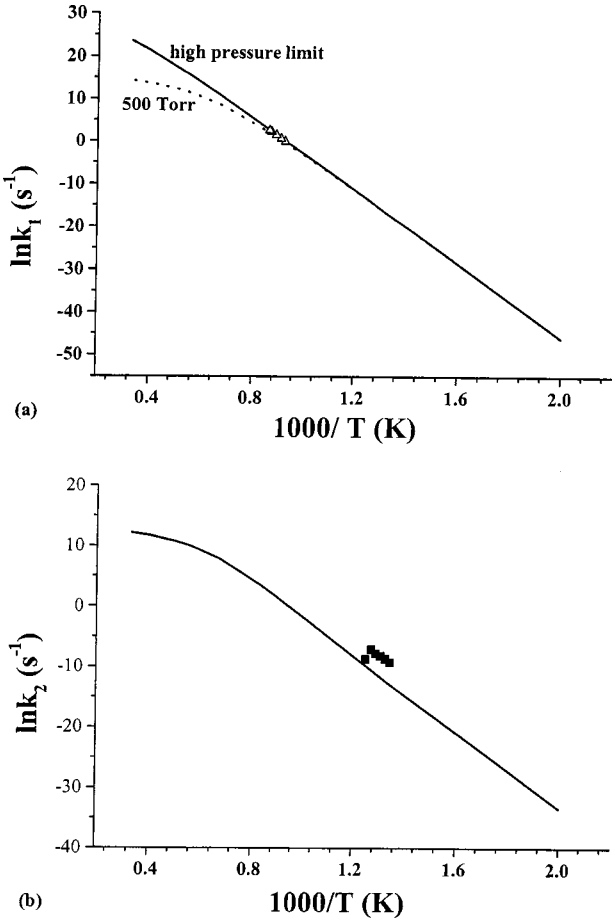

FIG. 5. Comparison of the predicted k_1 (a) and k_2 (b) under the corresponding experimental conditions. In (a), solid and dotted lines represent the calculated values at 500 Torr and the high-pressure limit, Δ, Ref. 4. In (b), solid line represents calculated values at 50 Torr: symbols are the experimental values obtained from the formation of C_3H_6 reported in Ref. 3 in the temperature range of 721–801 K and pressure between 10 and 100 Torr.

given in Fig. 2 and the moments of inertia and vibrational frequencies presented in Table II were used in the calculation.

Figures 3(a) and 3(b) show the rate constants predicted at 50 and 760 Torr, respectively. At 50 Torr, for the major channels, $k_2 > k_1 > k_4$ across the temperature range of 500–2500 K. For the minor channels, over 650 K, $k_6 > k_5 \approx k_3$, while under 650 K, $k_3 > k_5 \approx k_6$. Checking the energy diagram (Fig. 2), one can see that even though the energy barrier for channel (5), TS4, is higher than that of (3), TS2, by about 2.0 kcal/mol, both rate constants are very close at high temperatures. Similarly, the barrier of TS4 is larger than that of TS5 [channel (6)] by 2.4 kcal/mol: both k_5 and k_6 are close at the lower temperatures. The relative magnitudes of the rate constants at lower and higher temperatures shown in Fig. 3(a) may be attributed to the combined effects of their barriers and transition state structures (i.e., the enthalpies and entropies of the TS's). Figure 3(a) also shows that the formation of water and propene from channel (2) is considerably more important than the formation of H_2 and CH_4 by various molecular elimination channels, similar to that observed in the C_2H_5OH system because of the much lower dehydration barrier.[5] At 760 Torr [see Fig. 3(b)], the relative importance of $k_1 - k_6$ is similar to that predicted at 50 Torr, except that k_1 becomes slightly larger than k_2 over 1200 K.

Figures 4(a) and 4(b) plot the low- and high-pressure limit dissociation rate constants for channels (1)–(6), respectively. It is readily seen that at the low-pressure limit, the lowest barrier channel (2) is dominant due to its relatively low energy barrier; k_1^0, as expected, becomes the lowest one in the temperature range of 500–1200 K because of its large endothemicity, 87.0 kcal/mol. However, at the high-pressure limit, the order of $k_1 - k_6$ is similar to that predicted at 760 Torr.

Figures 5(a) and 5(b) compare the predicted and experimental rate constants for channels (1) and (2), respectively. The symbols in Fig. 5(a) are the experimental data from the work of Tsang[4] obtained at 398–503 Torr and in the temperature range of 1080–1160 K; the dotted and solid lines represent our predicted values at 500 Torr and at the high-pressure limit. The results show that below 1000 K, the dissociation rate constant for channel (1) at 500 Torr already reaches the high-pressure limit value; as expected, at higher temperatures, it shows a pressure dependence which is similar to the formation of $CH_3 + CH_2OH$ in the dissociation of C_2H_5OH.[5] The predicted values are in reasonable agreement with those of Tsang.[4] Figure 5(b) compares the predicted value of k_2 at 50 Torr with the experimental data of

TABLE IV. Equations for individual rate constants in units of s^{-1} predicted for different pressures.

	Lower-pressure limit[a]	50 Torr	760 Torr	Infinite pressure
k_1	$6.3\times10^{42}\,T^{-16.21}\exp(-47432/T)$	$1.6\times10^{81}\,T^{-19.56}\exp(-55921/T)$	$6.3\times10^{73}\,T^{-17.06}\exp(-55280/T)$	$8.0\times10^{29}\,T^{-3.75}\exp(-45841/T)$
k_2	$7.2\times10^{44}\,T^{-14.70}\exp(-35700/T)$	$1.6\times10^{51}\,T^{-11.46}\exp(-40423/T)$	$6.1\times10^{43}\,T^{-9.13}\exp(-39.186/T)$	$2.0\times10^{6}\,T^{2.12}\exp(-30667/T)$
k_3	$2.9\times10^{30}\,T^{-12.71}\exp(-32887/T)$	$3.2\times10^{57}\,T^{-14.01}\exp(-47395/T)$	$1.3\times10^{49}\,T^{-11.23}\exp(-46483/T)$	$7.7\times10^{-4}\,T^{4.58}\exp(-35173/T)$
k_4	$1.3\times10^{41}\,T^{-15.68}\exp(-41676/T)$	$8.5\times10^{70}\,T^{-17.23}\exp(-51761/T)$	$5.5\times10^{62}\,T^{-14.54}\exp(-50816/T)$	$2.2\times10^{13}\,T^{0.40}\exp(-40039/T)$
k_5	$1.4\times10^{33}\,T^{-13.63}\exp(-34252/T)$	$1.5\times10^{65}\,T^{-16.05}\exp(-50768/T)$	$9.6\times10^{56}\,T^{-13.29}\exp(-50042/T)$	$3.9\times10^{2}\,T^{3.20}\exp(-38391/T)$
k_6	$4.3\times10^{30}\,T^{-13.36}\exp(-38460/T)$	$8.2\times10^{73}\,T^{-18.24}\exp(-53832/T)$	$7.0\times10^{65}\,T^{-15.53}\exp(-53097/T)$	$1.2\times10^{13}\,T^{0.46}\exp(-41752/T)$

[a]Second-order rate constants are given in unit of $cm^3\,molecule^{-1}\,s^{-1}$.

Trenwith[3] obtained from the formation of C_3H_6 in the temperature range of 721–801 K and pressure between 10 and 100 Torr. The predicted values are lower than the experimental data by 1–2 orders of magnitude at the corresponding experimental temperatures, attributable to the contribution from the decomposition of the $CH_2C(H)OHCH_3$ radical formed in the chain reactions as proposed by Trenwith.[3]

In order to quantitatively account for Trenwith's experimental data, a detailed kinetic modeling is required. For future modeling applications, we have tabulated the individual rate constants predicted at various pressures in Table IV.

IV. CONCLUSION

The kinetics and mechanisms for the thermal decomposition of iso-C_3H_7OH have been investigated by high-level molecular orbital (G2M) and variational RRKM calculations over a wide range of reaction conditions. At pressures below 1 atm, the decomposition of iso-C_3H_7OH occurs primarily by the dehydration reaction producing $CH_3C(H)CH_2+H_2O$. At the high-pressure limit and over 1000 K, however, the production of $CH_3+CH_3C(H)OH$ becomes dominant and the decomposition reaction is controlled by chain processes. Different types of H_2- and CH_4-molecular elimination processes were found, but they are unimportant throughout the temperature range investigated. Our computed result for the formation of $CH_3+CH_3C(H)OH$ accounts well for Tsang's experimental results.[4,19]

ACKNOWLEDGMENTS

This work was supported in part to B.H.B. by the Department of Energy under Contract No. DE-FG05-91-ER14192 and in part to R.S.Z. and M.C.I. by the Office of Naval Research under Grant No. N0001402-0133. M.C.L. also acknowledges support by the Taiwan National Science Council for the Distinguished Visiting Professorship.

[1] J. A. Barnard, Trans. Faraday Soc. **56**, 72 (1960).
[2] A. Maccoll and P. J. Thomas, Prog. React. Kinet. **4**, 119 (1967).
[3] A. B. Trenwith, J. Chem. Soc., Faraday Trans. 1 **71**, 2405 (1975).
[4] W. Tsang, Int. J. Chem. Kinet. **8**, 173 (1976).
[5] J. Park, R. Zhu, and M. C. Lin, J. Chem. Phys. **117**, 3224 (2002).
[6] W. S. Xia, R. S. Zhu, M. C. Lin, and A. M. Mebel, Faraday Discuss. **119**, 191 (2001).
[7] J. Shu, J. J. Lin, Y. T. Lee, and X. Yang, J. Am. Chem. Soc. **123**, 322 (2001).
[8] A. M. Mebel, K. Morokuma, and M. C. Lin, J. Chem. Phys. **103**, 7414 (1995).
[9] A. D. Becke, J. Chem. Phys. **97**, 9173 (1992).
[10] A. D. Becke, J. Chem. Phys. **96**, 2155 (1992).
[11] A. D. Becke, J. Chem. Phys. **98**, 5648 (1993).
[12] C. Gonzalez and H. B. Schlegel, J. Chem. Phys. **90**, 2154 (1989).
[13] M. J. Frisch, G. W. Trucks, H. B. Schlegel *et al.*, GAUSSIAN 98, Gaussian, Inc., Pittsburgh, PA, 1998.
[14] S. J. Klippenstein, A. F. Wagner, R. C. Dunbar, D. M. Wardlaw, and S. H. Robertson, 1.00 ed. (1999).
[15] R. G. Gilbert and S. C. Smith, *Theory of Unimolecular and Recombination Reactions* (Blackwell Science, Oxford, 1990).
[16] K. A. Holbrook, M. J. Pilling, and S. H. Robertson, *Unimolecular Reactions*, 2nd ed. (Wiley, New York, 1996).
[17] M. Frenkel, G. J. Kabo, K. N. Marsh, G. N. Roganov, and R. C. Wilhoit, *Thermodynamics of Organic Compounds in the Gas State*, Trc Data Series (CRC, Baton Rouge, 1994).
[18] D. R. Lide and H. P. R. Frederikse, *CRC Handbook of Chemistry and Physics*, 78th ed. (CRC, Baton Rouge, 1997).
[19] W. Tsang, in *Shock Waves in Chemistry*, edited by A. Lifshitz (Marcel Dekker, New York, 1981) pp. 59–129.
[20] N. I. Butkovskaya, Y. Yhao, and D. W. Setser, J. Phys. Chem. **98**, 10779 (1994).
[21] S. Matzinger and M. P. Fuelscher, J. Phys. Chem. **99**, 10747 (1995).
[22] D. A. Modarelli, S. Morgan, and M. S. Platz, J. Am. Chem. Soc. **114**, 7034 (1992).
[23] J. S. Yadav and J. D. Goddard, J. Chem. Phys. **85**, 3975 (1986).
[24] M. Rasanen, T. Raaska, H. Kunttu, and J. Murto, THEOCHEM **67**, 79 (1990).
[25] F. M. Mourits and F. H. A. Rummens, Can. J. Chem. **55**, 3007 (1977).